Proceedings of Global Power and Propulsion Society
ISSN-Nr: 2504-4400
GPPS Xi'an21
18th – 20th October, 2021
www.gpps.global

GPPS-TC-2021-313

Compressor Tandem Cascade Flow Prediction by Adaptive POD-RBFN Reduced Order Model

Xun Shang
1. Yangtze River Delta Research Institute
2. Northwestern Polytechnical University
x.shang@mail.nwpu.edu.cn
Xian, Shaanxi, China

Hanru Liu*
1. Yangtze River Delta Research Institute
2. Northwestern Polytechnical University
hrliu@nwpu.edu.cn
Xian, Shaanxi, China

Yican Du
Northwestern Polytechnical University
duyican@mail.nwpu.edu.cn
Xian, Shaanxi, China

Zhijie Hu
Northwestern Polytechnical University
huzj@mail.nwpu.edu.cn
Xian, Shaanxi, China

ABSTRACT

The tandem cascade of compressor can perform larger flow turning angle and less losses than a single-row cascade. The Proper Orthogonal Decomposition (POD) was used in this paper to extract the dominant mode of the tandem flow field especially the gap injection between two blades. Radial Basis Function Network (RBFN) was used to respond to the coefficients of POD basis function for one Reduced-order-model (ROM) construction, so as to predict the flow field. It is concluded that the combined method can be utilized to accurately predict the aerodynamics parameters and flow field of tandem cascade. The adaptive sampling method was developed to further advance the sampling efficiency for ROM prediction. The result shows that the adaptive sampling method has obvious advantages compared with static sampling in terms of efficiency and accuracy.

INTRODUCTION

As a passive flow control technology, tandem blade have attracted the attention of a large number of researchers due to its simple structure and easy engineering application. As early as 1951, Spraglin conducted a preliminary theoretical study on the tandem cascade, calculating the two-dimensional incompressible ideal flow of the tandem cascade (Spraglin, 1951). Bammert and Staude studied the tandem rotor, and the results showed that the tandem blade clearance has a great influence on the blade losses and the pressure distribution on the blade surface (Bammert and Staude, 1980). Wang and Jin have studied the engineering applicability of tandem cascades (Wang, et al. 2006; Jin, et al. 2009). Liu et al. conducted a further study on the mechanism of the gap flow in the tandem cascade for flow modification, and the results showed that the gap flow effectively suppressed the suction surface separation of the rear blade, but had a smaller effect on the front blade (Liu, et al. 2018). To study the structure of blade-gap flow from the domain mode of the reduced-order model, the large-load tandem cascade was selected as the research object.

For fluid dynamics, CFD numerical simulation is often used to obtain the flow field structure. However, for the flow of complex structures, numerical simulation is particularly time-consuming, especially related to unsteady flow problem. In order to decrease the prediction cost, the reduced order model is commonly used by researchers to quickly determine the response of aerodynamic parameters or flow field. The POD method is an efficient dimensionality reduction method. This method can decompose a complex flow into different modal, among which the low-order modes contain the most information of the flow field. Therefore, it can be used for flow analysis or reduced order model (ROM) construction. The first application of the POD method in fluid mechanics was in turbulence analysis by Bakewell (Bakewell, et al. 1967). At present, this method has been widely used in the field of reduced-order model construction, such as the filling of missing data. Data filling is often realized by using the linear response of the POD basis function, which is GPOD, but

this method is not effective for strong nonlinear problems (Duan, at el. 2012). RBFN is a way to solve this problem. The main idea of the POD-RBFN hybrid model is to use POD decomposition to obtain the fundamental mode of the flow field, and then use the radial basis function neural network to respond to the coefficients of the fundamental mode, and finally realize the prediction of the missing sample flow field (Kato and Funazaki, 2014).

To construct the POD-RBFN hybrid model, the quality and quantity of the initial samples have a great influence on the model reconstruction accuracy. The adaptive sampling method based on function response deviation has been developed rapidly in recent years (Braconnier, et al. 2011). Therefore, in order to improve the sampling efficiency and the reconstruction accuracy of the reduced-order model, the adaptive sampling method was also studied in the present paper.

METHODOLOGY

Research Object & Numerical Methodology

The high-load two-dimensional compressor tandem cascade was numerical researched in this paper (Eckel, et al. 2016). Table 1 presents the main design geometric parameters of the cascade.

Table 1 Geometric parameters of tandem cascade

Parameters	Front blade	Rear blade
Chord c /mm	31.50	31.50
Bending angle θ /°	24.50	51.50
Installation angle γ /°	39.40	10.80
Geometry inlet angle β_{1k} /°	33.39	
Overall chord c /mm	62.40	
Pitch t /mm	32.64	
Axial overlap (AO)	0.01	
Percent pitch (PP)	0.91	

The calculating grid was generated using AutoGrid 5 and the H-O-H structured grid topology was adopted for two blades. The grid width of the first layer was 1×10-6 m and y+ was limited under 1. The total grid number of the two-dimensional calculation domain was 39896. Figure 1 demonstrated the schematic diagram of the single-channel grid set and the topology at the gap of two blade.

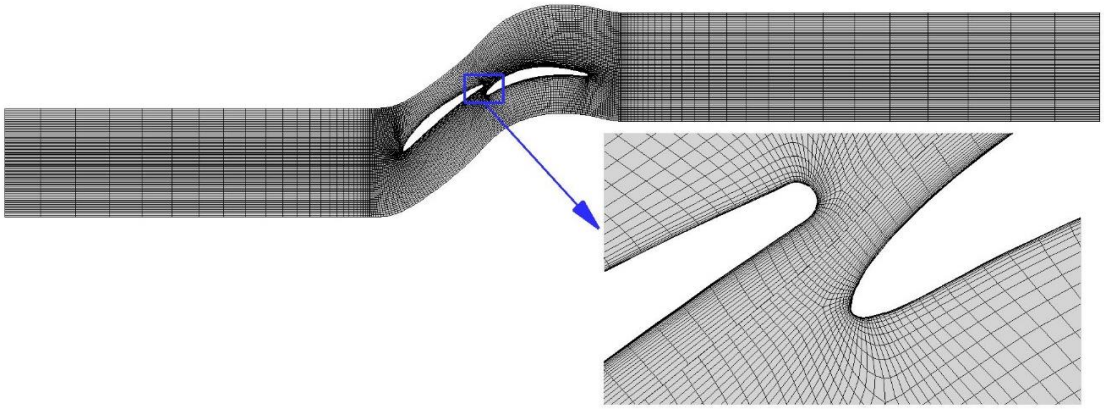

Figure 1 Schematic Diagram of Single-channel Grid

The steady and unsteady compressible Reynolds average N-S equations were solved numerically in a single passage domain by using CFX. The SST turbulence model with $\gamma - \mathrm{Re}_\theta$ transitional model was employed to calculate the turbulent viscosity. The end-wall were set as non-slip wall. The inlet total temperature and total pressure were 288.15 K and 101325 Pa respectively. The inlet Mach number $Ma_{in} = 0.6$ is obtained by adjusting the outlet average static pressure gradually. The unsteady physical time step is 2×10^-5 s.

POD-RBFN Surrogate Model

The singular value decomposition of early POD requires all the solutions in the domain, and it performs poorly in solving eigenvalues and system stability, which limits its application in engineering. With the introduction of the snapshot POD method (Sirovich and Kirby, 1987), the calculation volume and stability problems have been improved,

it's therefore the POD method has gradually been applied in various fields. The basic process of snapshot POD is as follows.

The first step is to obtain a snapshot matrix $U=[u_1\ u_2\ ...\ u_n]$ based on a set of solutions of the system, and decentralize the matrix:

$$V=U-\overline{U} \tag{1}$$

Where the $\overline{U}$ is the snapshot mean matrix and the V is the snapshot pulsation matrix.

The core work of the POD method is to find a set of optimal orthogonal basis $\Phi=[\phi_1\ \phi_2\ ...\ \phi_n]$ and the corresponding basis coefficient matrix $A=[a_1\ a_2\ ...\ a_n]$, so that it satisfies:

$$v_i=a_i\phi_i \tag{2}$$

The optimal orthogonal basis of the snapshot pulsating matrix can be obtained by solving the following optimal value problem:

$$Min:\|V-\Phi A\|_2 \tag{3}$$

Singular value decomposition is used to solve the optimal value problem, so as to obtain the optimal POD basis Φ. Then map the snapshots of each flow field to Φ, and then obtain the basis coefficients corresponding to each flow field

According to the definition of fundamental mode "energy" (Sirovich, 1987), if the fundamental modes are sorted, the first few modes contain most of the "energy" in the flow field. Therefore, the low-order reconstruction of the original flow field can be realized by using less modal order. The "energy" of a certain order fundamental mode is defined as:

$$E_i=\frac{\lambda_i}{\sum\lambda_i} \tag{4}$$

Where λ_i is the i-th eigenvalue of autocorrelation matrix $R=V^{\mathrm{T}}V$.

After the optimal POD basis is obtained, the original flow field can be accurately reconstructed according to the coefficient matrix A and equation (2). Therefore, if the coefficient vector corresponding to the non-original sample flow field can be obtained, the non-original sample flow field can be predicted and reconstructed based on the known POD basis. In order to predict the POD coefficients of the non-sample flow field, and then reconstruct the prediction and reconstruction of the non-sample flow field, the radial basis function neural network is introduced in this paper. Radial Basis Function Neural Network (RBFN) is a neural network proposed by Broomhead and Lowe that has fast convergence, simple structure, and uniform approximation to nonlinear systems (Broomhead and Lowe, 1988). RBFN is a classic three-layer forward network. The first layer is the input layer, the second layer is the hidden layer, and the third layer is the output layer. The hidden layer uses the radial basis function as the neuron of the activation function.

Adaptive Sampling

In order to solve the problem of the sample's influence on the reconstruction accuracy and stability of the flow field, an adaptive sampling method based on the deviation of the function response is used in this paper. The basic principle of the "Quad Trees" method is (Finkel, et al. 1984): the first step is to extract boundary corner sample points, center sample points, and subspace center sample points in the sample space. Then the target subspace is determined by calculating the function response deviation of these several sample points. Next, the center point of the next-generation subspace of the target subspace is added to the sample set. Re-determine the target subspace in the new sample set and add new sample points. Repeat the previous step until the final response deviation of all sampling points meets the requirements or the total number of samples meets the requirements.

The function response deviation value in this process is obtained by the following formula:

$$F(u_i)=D(u_i)E(u_i) \tag{5}$$

In this formula, $E(u_i)$ is the response deviation of the i-th flow field snapshot u_i, $D(u_i)$ represents the correlation between the i-th flow field sample u_i and other samples, which is determined by the following formula:

$$D(u_i)=\frac{1}{n-1}\sum(1-\rho_{ij}) \tag{6}$$

In this formula, n is the total number of samples. ρ_{ij} represents the linear correlation coefficient between the i-th sample flow field and the j-th sample flow field. This formula calculates the mean value of the correlation between the sample flow field u_i and other sample flow fields. The stronger the correlation is, the smaller the $D(u_i)$ is.

The response deviation $E(u_i)$ is obtained by cross-validation of "Leave-One-Out" (LOO) (Meckesheimer, 2002). The basic principle of this method is: first remove the sample snapshot u_i from the initial snapshot set. Then predict the missing sample u_i based on the remaining samples. The overall error of the predicted flow field is the response deviation $E(u_i)$.

RESULTS AND DISCUSSION

CFD evaluation of tandem cascade

Before the unsteady calculation and subsequent analysis, the aerodynamic characteristics of the tandem cascade are first evaluated, so as to provide a reference for determining the working conditions of the following study.

The calculation stations are set up at the cross section at the inlet one time of chord length and the outlet 0.5 time of chord length respectively. Figure 2 shows the pressure ratio and cascade losses characteristic diagram of the tandem cascade. The left vertical axis Pr is the static pressure ratio of the cascade, and the right vertical axis is the cascade loss coefficient. It can be seen from the figure that as the incidence of the inlet airflow increases, the static pressure ratio of the cascade increases first and then decreases sharply. The change trend of the cascade loss coefficient is roughly opposite to that of Pr. This is reasonable. As the incidence increases, the blade basin separation flow gradually weakens, so the static pressure ratio gradually increases and the loss gradually decreases. When the incidence of the airflow increases further, airflow separation occurs on the back of the blade, which causes the flow field to deteriorate sharply, the static pressure ratio decreases sharply, and the loss increases sharply.

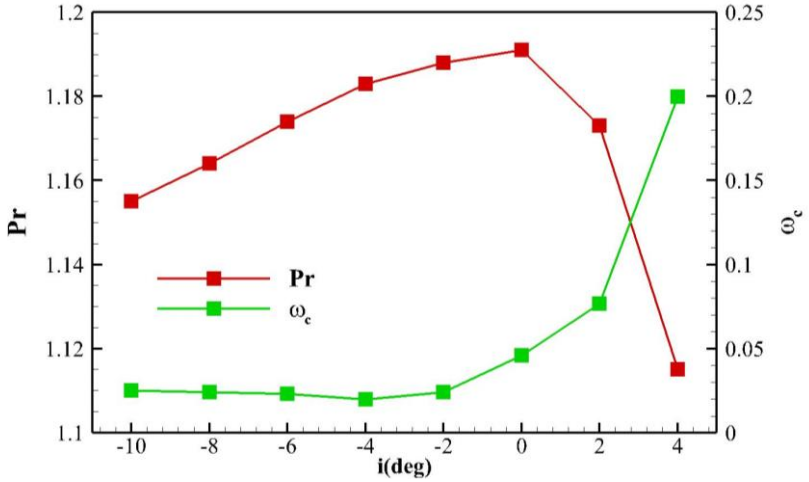

Figure 2 Incidence Characteristic of Tandem Cascade

In order to research the unstable flow characteristics of the separated flow, the 2° angle of attack condition is selected in this paper for the unsteady simulation and the subsequent processing analysis.

Figure 3 shows the Mach number field and streamline distribution of the flow field near the blade. It can be seen from the figure that, under a larger air attack angle, a wide range of blade back separation flow mainly occurs on the front blade. This is because, on the one hand, compared with the conventional single-row cascade, the chord length of a single tandem cascade front blade is shorter and the airflow turning angle is larger, which makes the front blade easier to separate. On the other hand, due to the blade-gap flow, the low-energy fluid generated by the separation of the front blade trailing edge is not easily mixed with the airflow of the rear blade, which makes the separation of the front blade more serious. Contrary to the front blade, due to the blowing effect of the tandem cascade blade-gap flow, the rear blade is always in a relatively stable flow condition, so no obvious separation flow occurs.

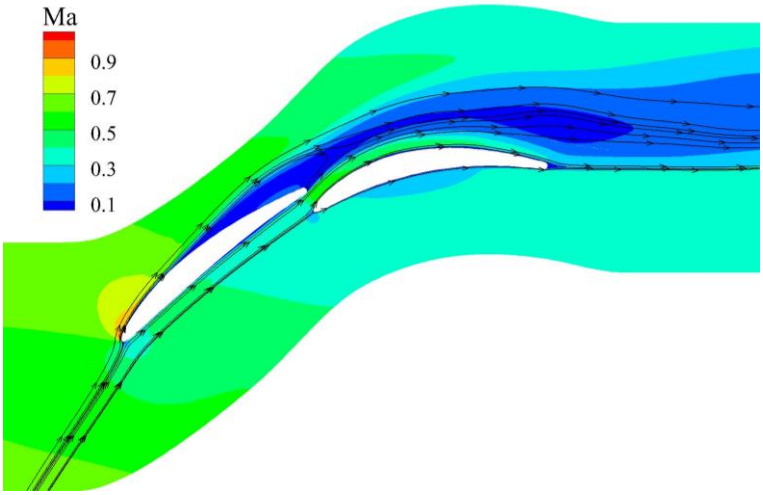

Figure 3 Mach Number and Sreamline Distribution

Proper Orthogonal Decomposition

The flow field of 100 continuous time steps obtained by unsteady calculation is selected as the original sample flow field set. The flow field vorticity distribution is extracted, and construct a flow field snapshot matrix. Each column in the snapshot matrix represents the flow field vorticity distribution at a time step, so there are 100 columns in the matrix. Perform POD decomposition on the flow field snapshot matrix to obtain the corresponding POD basis functions and the corresponding POD coefficients.

Solve the eigenvalues of the autocorrelation matrix *R*, and sort the eigenvalues. Then according to formula (4), the proportion of "energy" of each POD fundamental mode can be obtained. Therefore, it can be determined which modes can contain most of the information in the original flow field.

Table 2 shows the energy ratio of the first 10 POD fundamental modes and the total energy ratio of the first *n* modes. Figure 4 shows the variation trend of the energy of each POD fundamental mode. In the figure, the abscissa denoted the POD mode, and the ordinate is the proportion of energy in the logarithmic form.

Table 2 The energy proportion of each mode

Mode	1	2	3	4	5	6	7	8	9	10
E_i (%)	41.02	16.41	12.37	9.54	4.22	3.43	2.20	1.85	1.73	1.18
$\sum E_i$ (%)	41.02	57.43	69.81	79.35	83.57	87.00	89.20	91.06	92.78	93.96

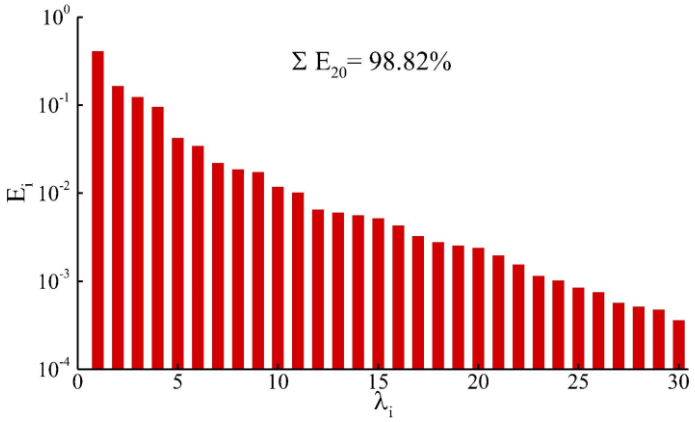

Figure 4 Energy Distribution of Each POD Mode

It can be seen from Table 2 and Figure 4 that the energy proportion of each mode after the 8th order is less than 2%. In addition, the energy proportion of the first 10 modes reaches 93.96%, so the flow field reconstructed from the first 10 fundamental modes can already contain most of the information in the flow field.

Figure 5 shows the cloud chart of POD modes. It can be seen that the POD fundamental mode vortex core structure alternates between positive and negative along the flow direction. In addition, the fluctuations of the front blade separation vortex and shedding vortex structure are significantly stronger than those of the rear blade, occupying most of the vortex energy in the flow field. Due to the blade-gap flow, the interference between the front blade shedding vortex and the rear blade separation vortex is hindered, thereby avoiding the enhancement of the rear blade separation vortex. Therefore, the rear blade can maintain a better flow state even at a larger angle of incidence.

The distance between adjacent vortex core structures in the high-order mode cloud chart is reduced, which indicates that the high-order mode captures the smaller-scale vortex structure in the tandem cascade flow field. The interaction and influence between vortex cores are also more complicated.

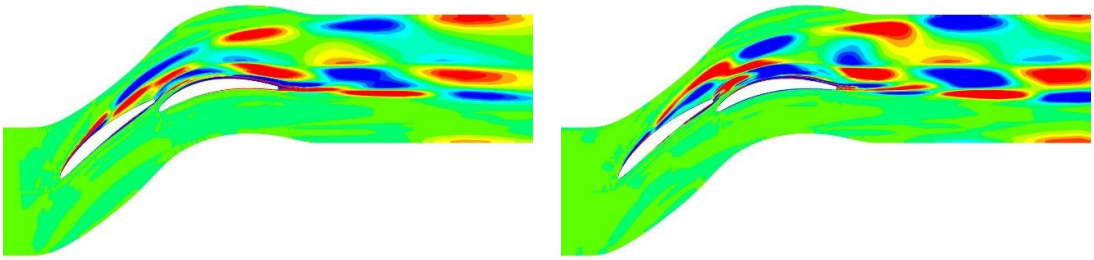

Mode 1 Mode 3

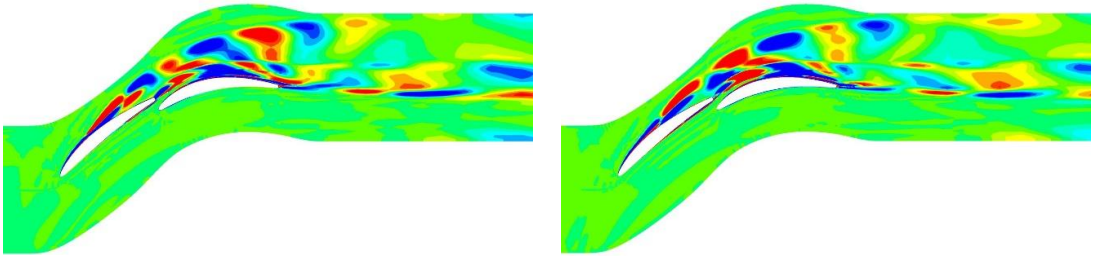

Mode 5 Mode 7

Figure 5 Each POD Mode Cloud Chart

Figure 6 shows the original flow field vorticity cloud chart at time step t=1 and the vorticity cloud chart reconstructed using low-order modes. It can be seen that the flow field reconstructed using the first 4 POD fundamental modes can already reflect most of the flow structure of the original flow field. The reconstructed flow field of the first 8 fundamental modes is only slightly different from the original flow field. As the modal order is further increased, the expression of the original flow field's fine structure by the reconstructed flow field is also clearer. This result is consistent with the conclusion drawn above based on the proportion of modal energy.

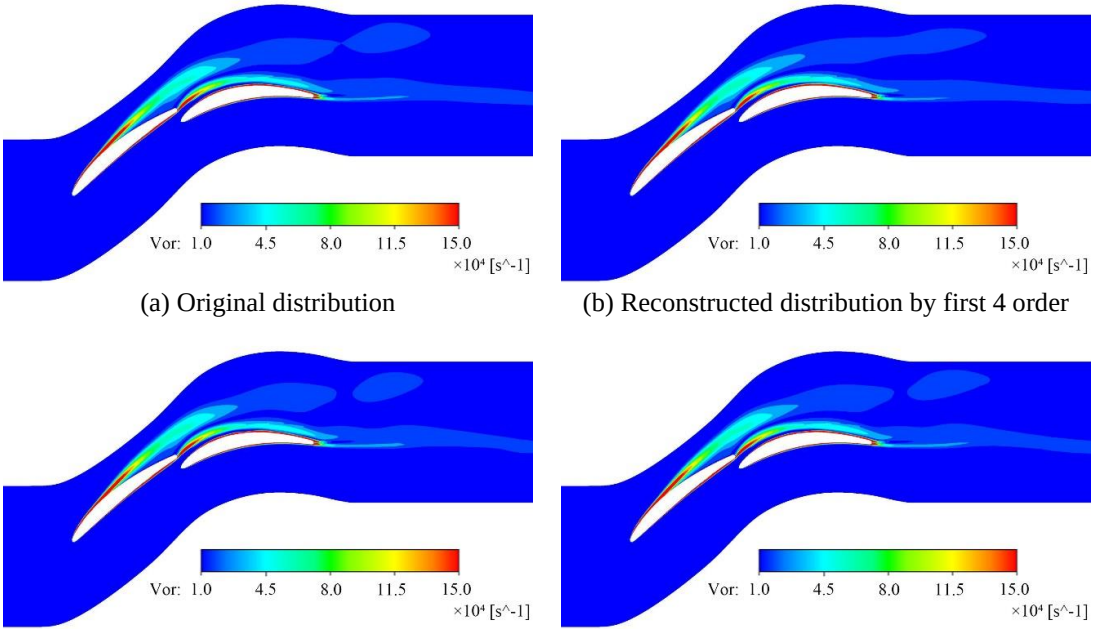

(a) Original distribution (b) Reconstructed distribution by first 4 order

(c) Reconstructed distribution by first 8 order (d) Reconstructed distribution by first 20 order

Figure 6 Original & Reconstructed Vorticity Distribution

Flow Field Reconstruction by POD-RBFN

The Mach number distribution of the flow field for 100 consecutive time steps is taken as the original sample space. Randomly sample 60 samples to form a flow field snapshot matrix, which is used to obtain the POD fundamental mode and the corresponding coefficients. Then, the time step is taken as input, and the POD modal coefficients are taken as output to construct an RBF neural network proxy model. The prediction of the POD modal coefficients of the non-sample flow field is realized.

The POD-RBFN hybrid model is used to predict and reconstruct the non-sample flow field, and the overall reconstruction error of the flow field is defined as:

$$\varepsilon_m = \frac{1}{N}\sum_{i=1}^{N}\left(Ma_{mi} - Ma_{moi}\right) \tag{7}$$

Where N is the number of nodes in the Mach number distribution cloud chart. Ma_{mi} is the local Mach value of the i-th flow field node in the reconstructed flow field. Ma_{moi} is the local Mach value of the i-th node in the original flow field.

Different modal orders are used to predict and reconstruct the flow field at time t=56 (non-sample flow field), and the relationship between the overall reconstruction error and the modal order is obtained, as shown in Figure 7. It can be seen that when the modal order is small, the reconstruction error decreases sharply with the increase of the modal order.

But when the modal order is greater than 22, the magnitude of the reconstruction error changes with the increase of the modal order is small. This is because the first 20 fundamental modes already contain more than 98% energy of the flow field, so higher-order modes have little effect on the flow field reconstruction.

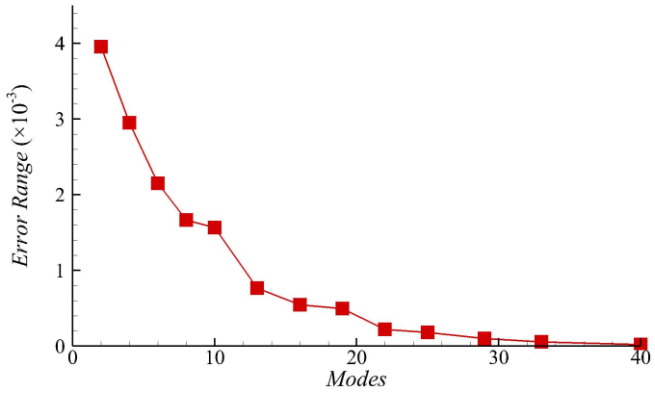

Figure 7 Overall Reconstruction Error with Different Modes

Figure 8 shows the results of predictive reconstruction flow field at t=56 (non-sample flow field) using the first 10 modes, and Figure 9 shows the reconstruction error distribution. It can be seen that the Mach number distribution reconstructed using the first 10 modal predictions is only slightly different from the original flow field. The reconstruction error of the flow field is mainly distributed at the positions of the separation vortex and the shedding vortex core of the front and rear blade. This is due to the mutual interference and evolution of the vortex structure, which makes the flow in this area more complex and changeable, resulting in lower reconstruction accuracy

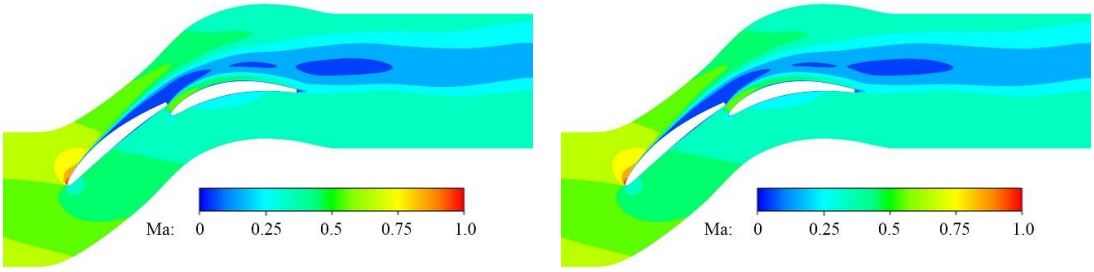

(a) Original distribution (b) Reconstructed distribution

Figure 8 Mach Number Distribution

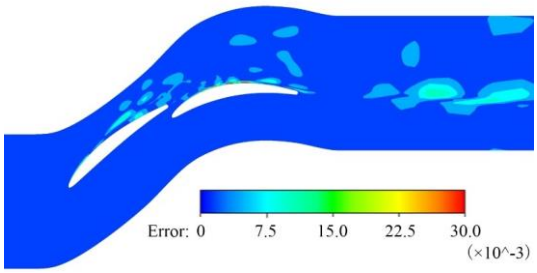

Figure 9 Reconstruction Error Distribution

Flow Field Reconstruction with Adaptive Sampling

The POD-RBFN hybrid model is constructed in this paper needs some initial samples. Therefore, firstly extract 11 samples from 100 flow field snapshots at equal intervals as the initial samples for adaptive sampling. Then the "Quad Trees" method based on the deviation of the function response is used for adaptive sampling. The adaptive sampling object is a one-dimensional time step sequence, two new sample points will be obtained after each sampling, and a total of 20 adaptive samplings are performed.

The sample points obtained by adaptive sampling and random sampling are used to predict and reconstruct the flow field at random 25 time steps, and the average value of the reconstruction error is calculated. Figure 11 shows the relationship between the average reconstruction error and the number of samples. It can be seen that after adaptive sampling, the accuracy of flow field reconstruction and the number of samples required are better than static random

sampling. For example, the reconstruction accuracy of 43 sample points in adaptive sampling in the figure is approximately the same as that with 60 samples in random sampling. When the number of samples is the same, the reconstruction error of adaptive sampling is significantly lower than that of static random sampling.

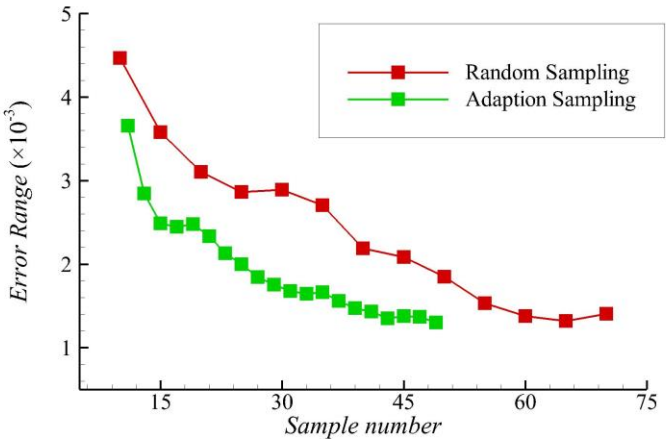

Figure 11 Reconstruction Error Comparison

Using adaptive sampling and random sampling to obtain 45 samples, respectively, the Mach number distribution of the flow field at the 92nd time step (non-sample time step) is predicted. Figure 12 shows the error distribution cloud chart reconstructed by the two sampling methods. It can be seen that the adaptive sampling method obviously reduces the reconstruction error in the occurrence and development area of the vortex structure, especially in the downstream wake of the blade, thereby improving the overall reconstruction accuracy of the flow field.

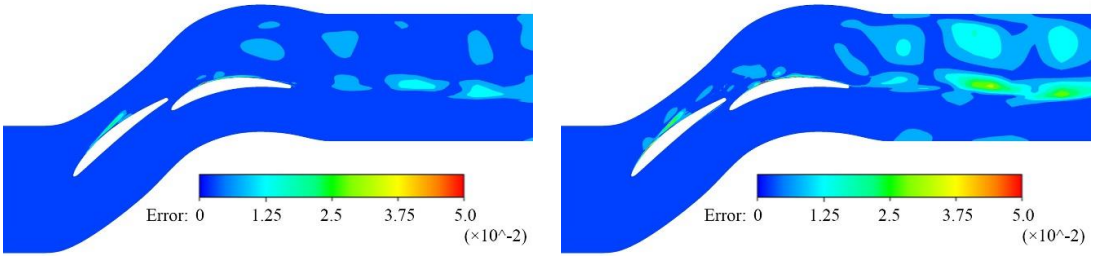

(a) Adaptive sampling (b) Random sampling

Figure 12 Comparison of Reconstruction Error Distribution

CONCLUSIONS

The flow field structure of the large turning angle tandem cascade is numerical analyzed in this paper and it shows that the tandem cascade gap flow blows off the low-energy fluid on the suction surface of the rear blade, and suppresses the interference effect of the front blade shedding vortex on the rear blade. This makes the rear blade work under a good flow condition, so that the tandem cascade can obtain a larger airflow turning angle with a smaller cascade loss.

The POD method is used to decompose the unsteady flow field of the tandem cascade to obtain the POD fundamental modes and the corresponding modal coefficients. According to the energy proportion of each fundamental mode, the first few fundamental modes contain most of the information of the flow field. Then, it was verified by reconstructing the original flow field using low-order modes. In addition, the tandem cascade flow field is analyzed from the perspective of the POD mode. It is found that the low-order mode mainly contains the information of the large-scale vortex structure in the flow field, while the high-order mode reflects the small-scale vortex structure. The gap flow of the tandem cascade mainly suppresses the interference between the front blade shedding vortex and the rear blade separation vortex, so that the rear blade can maintain a good flow condition.

By constructing the RBFN to respond to the modal coefficients of the non-sample flow field, the prediction and reconstruction of the non-sample flow field are realized. The results show that the POD-RBFN reduced-order model can accurately predict and reconstruct the missing flow field, and the reconstruction accuracy is affected by the number of samples and fundamental modes.

In order to improve the sampling efficiency of the reduced-order model and improve the sample utilization, an adaptive sampling method based on the deviation of the function response is used in this paper. Sampling reconstruction results show that compared with static random sampling, the adaptive sampling method has obvious advantages in both the number of samples required and the reconstruction accuracy.

ACKNOWLEDGMENTS

The authors would like thank the National Science and Technology Major Project of China (No. 2017-II-0009-0023) and the Taicang City Innovation Leading Special Project (No. TC2019DYDS09) for supporting the research work.

REFERENCE

Bakewell, H., and Lumley, J. (1967). Viscous Sublayer and Adjacent Wall Region in Turbulent Pipe Flow. *The Physics of Fluids*, 10 (9): 1880-1889.

Bammert, K., and Staude, R. (1980). Optimization for Rotor Blades of Tandem Design for Axial Flow Compressors. *Journal of Engineering for Power*, 102(2): 369-375.

Braconnier, T., Ferrier, M., Jouhaud, J., et al. (2011). Towards an Adaptive POD/SVD Surrogate Model for Aeronautic Design. *Computers & Fluids*, 40(1):195-209.

Broomhead, D., and Lowe, D. (1988). Multi-variable Functional Interpolation and Adaptive Networks. *Complex Syst*, 2, 327-355.

Duan, Y., Cai, J., and Li, Y. (2012). Gappy Proper Orthogonal Decomposition-Based Two-Step Optimization for Airfoil Design. *AIAA Journal*, 50(4), 968-971.

Eckel, J., Heinrich, A., Janke, C., et al. (2016). 3D Numerical and Experimental Investigation of High Turning Compressor Tandem Cascade. *Deutscher Luft- und Raumfahrtkongress* 2016.

Finkel, R., Bentley, R., and Jon, L. (1984). Quad Trees: A Data Structure for Retrieval on Composite Keys. *Acta Informatica*, 4(1), 1-9.

Jin, H., Ye, Z., and Gong, J. (2009). Test of the characteristics of axial flow compressor with splitter. *Journal of Aerospace Power*, 24(8): 1813-1817.

Kato, H., and Funazaki, K. (2014). POD-Driven Adaptive Sampling for Efficient Surrogate Modeling and its Application to Supersonic Turbine Optimization. *ASME Turbo Expo 2014: Turbine Technical Conference and Exposition.*

Liu, H., Yue, S., Wang, Y., et al. (2018). Research on the Effect of Slotted Jet in Tandem Cascade on Separation Flow and Cascade Performance. *Journal of Propulsion Technology*, 39(12): 2728-2736.

Meckesheimer, M., Booker, A., Barton, R., et al. (2002), Computationally Inexpensive Metamodel Assessment Strategies. *AIAA Journal*, 40(10), 2053–2060.

Sirovich, L. (1987). Turbulence and the Dynamics of Coherent Structures, Part I: Coherent Structures. *Quarterly of Applied Mathematics*, 45 (3): 561-571.

Sirovich, L., and Kirby, M. (1987). Low-Dimensional Procedure for the Characterization of Human Faces. *J. Opt. Soc. Am. A*, 4 (3): 519-524.

Spraglin, W. (1951). Flow through cascades in tandem. *Quarterly Journal of Mechanics & Applied Mathematics*, 8(3):280-292.

Wang, H., Jiang, H., and Chen, M. (2006). Experimental Investigation of Splitter Compressors in a Planer Cascade. *Journal of Engineering Thermophysics*, 27(1): 113-116.